Available online at www.sciencedirect.com

SCIENCE DIRECT

Biochimica et Biophysica Acta 1668 (2005) 175–189

BIOCHIMICA ET BIOPHYSICA ACTA BBA

http://www.elsevier.com/locate/bba

The interactions of antimicrobial peptides derived from lysozyme with model membrane systems☆

Howard N. Hunter[a,1], Weiguo Jing[a,1], David J. Schibli[a], Tony Trinh[a], In Yup Park[b], Sun Chang Kim[b], Hans J. Vogel[a,*]

[a]*Structural Biology Research Group, Department of Biological Sciences, University of Calgary, Calgary, Alberta, Canada T2N 1N4*
[b]*Department of Biological Sciences, Korea Advanced Institute of Science and Technology, 373-1 Yusong-gu, Kusong-dong, Taejon 305-701, Korea*

Received 5 July 2004; received in revised form 2 December 2004; accepted 7 December 2004
Available online 29 December 2004

Abstract

Two peptides, RAWVAWR-NH_2 and IVSDGNGMNAWVAWR-NH_2, derived from human and chicken lysozyme, respectively, exhibit antimicrobial activity. A comparison between the L-RAWVAWR, D-RAWVAWR, and the longer peptide has been carried out in membrane mimetic conditions to better understand how their interaction with lipid and detergent systems relates to the reported higher activity for the all L-peptide. Using CD and 2D ^{1}H NMR spectroscopy, the structures were studied with DPC and SDS micelles. Fluorescence spectroscopy was used to study peptide interactions with POPC and POPG vesicles and DOPC, DOPE, and DOPG mixed vesicle systems. Membrane–peptide interactions were also probed by ITC and DSC. The ability of fluorescein-labeled RAWVAWR to rapidly enter both *E. coli* and *Staphylococcus aureus* was visualized using confocal microscopy. Reflecting the bactericidal activity, the long peptide interacted very weakly with the lipids. The RAWVAWR-NH_2 peptides preferred lipids with negatively charged headgroups and interacted predominantly in the solvent–lipid interface, causing significant perturbation of membrane mimetics containing PG headgroups. Peptide structures determined by ^{1}H NMR indicated a well-ordered coiled structure for the short peptides and the C-terminus of the longer peptide. Using each technique, the two enantiomers of RAWVAWR-NH_2 interacted in an identical fashion with the lipids, indicating that any difference in activity in vivo is limited to interactions not involving the membrane lipids.

Keywords: Lysozyme; Antimicrobial peptide; Phospholipid; Membrane mimetic; Structure

1. Introduction

Over the last decade, the search for antibacterial agents has seen rapid growth with the discovery of numerous naturally occurring antimicrobial peptides. From the analysis of these unique peptides, the focus of much research has been centred upon exploiting the properties that selectively kill bacteria while leaving eukaryotic cells

Abbreviations: 1D, one dimensional; 2D, two dimensional; CD, circular dichroism; CFU, colony forming unit; CSI, chemical shift index; DSC, differential scanning calorimetry; nuclear magnetic resonance; DSS, sodium 3-(trimethylsilyl)-1-propanesulfonate; DPC, dodecylphosphocholine; DPPG, 1,2-dipalmitoyl-*sn*-3-phosphatidylglycerol; DPPC, dipalmitoylphosphatidylcholine; DPPE, dipalmitoylphosphatidylethanolamine; DO, dioleoyl; DOPC, dioleoylphosphatidylcholine; DOPG, dioleoylphosphatidylglycerol; DOPE, dioleoylphosphatidylethanolamine; HPLC, high performance liquid chromatography; ITC, isothermal titration calorimetry; LUVs, large unilamellar vesicles; MLVs, multilamellar vesicles; NAPB, sodium phosphate buffer; NMR, nuclear magnetic resonance; NOE, nuclear Overhauser effect; NOESY, nuclear Overhauser enhancement spectroscopy; PC, phosphatidylcholine; PE, phosphatidylethanolamine; PO, 1-palmitoyl-2-oleoyl; POPC, 1-palmitoyl-2-oleoyl-*sn*-glycero-3-phosphocholine; POPG, 1-palmitoyl-2-oleoyl-*sn*-glycero-3-[(phospho-rac-(1-glycerol)] (sodium salt); rmsd, root-mean-square deviation; SDS, sodium dodecyl sulfate; TOCSY, total correlation spectroscopy

☆ This work was supported by an operating grant from the Canadian Institutes for Health Research (CIHR) to H.J.V. H.J.V. holds a Senior Scientist Award from the Alberta Heritage Foundation for Medical Research (AHFMR), while W.J. holds an AHFMR postdoctoral fellowship award.

* Corresponding author. Tel.: +1 403 220 6006; fax: +1 403 289 9311.
E-mail address: vogel@ucalgary.ca (H.J. Vogel).

[1] These authors contributed equally to this work.

0005-2736/$ - see front matter © 2004 Elsevier B.V. All rights reserved.
doi:10.1016/j.bbamem.2004.12.004

unaffected [1]. To this end, a significant effort has been directed towards the understanding of specific interactions that enhance the bactericidal properties of a peptide [2–7]. Although antimicrobial peptides have been isolated from various species, many human sources of innate and putative antimicrobial peptides are continuously being discovered [8]. A novel branch of this work involves the discovery of antimicrobial peptides released upon the digestion or breakdown of proteins. Two examples are lactoferricin released from lactoferrin (for a recent review, see [9]) and various lysozyme peptides released from the proteolytic digest of lysozyme [10]. Other examples concern antimicrobial peptides from hemoglobin [11] or cathepsin [12].

Lysozyme has long been known for having the ability to disrupt many bacterial functions, including membrane structure [10,13–16]. This activity is not always related to its enzymatic activity; for example, inactivated lysozyme and specific peptides isolated from proteolytic digests of hen egg white lysozyme have been shown to exhibit antimicrobial activity against both Gram positive and Gram negative bacteria [10,17]. One of the peptides studied (IVSDGNGMNAWVAWR residues 98–112, see Fig. 1) was isolated and found to have varied activity. Yet, a refined search of the key portions exhibiting activity revealed that not all segments of this peptide retained antimicrobial properties. Ile98–Met105 was inactive while Asn106–Arg112 was weakly active. Furthermore, the C-terminal portion NAWRAWR showed improved antimicrobial activity by exchanging Asn with Arg. This modified segment corresponds to residues 107–113 of human lysozyme (see Fig. 1). In the earlier report, the natural all L-RAWVAWR peptide was more active than the synthetic all D-RAWVAWR peptide against *Serratia marcescens*, *Micrococcus luteus*, *Staphylococcus aureus*, *Staphylococcus epidermidis*, and *Staphylococcus lentus* [10]. These observations seemingly contradict many studies reporting that the replacement of L- with D-amino acids actually made little difference or created enhanced resistance to enzymatic degradation, thereby increasing the activity of the all D-peptides over all L-peptides (e.g. [18,19]). Other key aspects of this study were elucidated from specific amino acid substitutions in the peptide and indicated the necessity of two Arg as well two Trp residues for the peptide to maintain activity [10]. The notion that many peptides containing at least two Arg and two Trp have potent antimicrobial activity has recently been reviewed [9,20].

A Hen lysozyme

98 112

I V S D G N G M N A W V A W R

B V V R D P Q G I **R A W V A W R**

99 113

Human Lysozyme

Fig. 1. Amino acid sequences for hen lysozyme (A) and human lysozyme (B). Residues in bold are the subject of this study.

More recently, the scope of activity of the lysozyme-derived peptides was expanded to include the larger helix–loop–helix sections from chicken (Asp87–Arg114) and human (Asp87–Arg115) lysozyme in order to compare activity and membrane permeabilization [13]. This larger section of lysozyme also presented a wide range of bactericidal activity against both Gram positive and Gram negative bacteria. The most active segments in these studies were shown to be either the full helix–loop–helix or the latter sections Ala107–Arg114 in chicken and Arg107–Arg115 in human lysozyme. In both cases, the activity of the peptides centres around the cationic Trp containing segment (R)AWVAWR(NR).

Our current work involves a study of the longer peptide IVSDGNGMNAWVAWR-NH_2 from chicken lysozyme and the shorter, more active peptide RAWVAWR-NH_2 from human lysozyme, as well as a comparison between the L- and all D-forms of RAWVAWR-NH_2. These peptides have been studied under membrane mimetic conditions either with micelles or vesicles to obtain more detailed information regarding membrane binding and the resulting peptide secondary structure. We have combined ^{1}H NMR, fluorescence, CD, DSC, and ITC to provide a comprehensive and detailed analysis of the lysozyme peptide interactions with a variety of lipids with different headgroups. To complement these studies and put the peptide interactions in perspective of the overall cell penetration capabilities, we have also studied the location of fluorescein labeled peptides in both *E. coli* and *S. aureus*.

2. Methods and materials

2.1. Materials

The synthetic peptides RAWVAWR (L), RAWVAWR (D), and IVSDGNGMNAWVAWR (L) were synthesized at the peptide synthesis facility at the University of Waterloo (Waterloo, ON). All three peptides were amidated on the C-terminal end to remove the negative charge. DPPC, DPPG, DOPC, DOPE, DOPG, POPC, and POPG dissolved in chloroform were purchased from Avanti Polar Lipids (Alabaster, AL) and were used without further purification. Sodium dodecyl-d_{25} sulfate (SDS), dodecylphosphocholine-d_{38} (DPC), and D_2O were purchased from Cambridge Isotopes Laboratories, Inc. (Andover, MA). Sodium 2,2-dimethyl-2-silapentane-5-sulfonate (DSS) was purchased from MSD isotopes. Acrylamide and Tris were purchased from ICN Biomedicals Inc. (Aurora, OH). HEPES and MES were purchased from Sigma Chemical Co. (St. Louis, MO), and citric acid and NaCl were purchased from BDH Inc. (Toronto, ON). The N-terminally labeled fluorescein peptide RAWVAWR-NH_2 was purchased from UVic Protein Chem-

istry Centre (Victoria, British Columbia) and used without further purification.

2.2. Preparation of multilamellar and unilamellar vesicles

Multilamellar lipid vesicles for DSC experiments were prepared in the following manner. Appropriate amounts of DPPG and DPPC stock solution were dried over a stream of nitrogen gas and stored over vacuum overnight to remove trace amounts of organic solvent. The dried lipid films were then dispersed in excess buffer (20 mM phosphate, 130 mM NaCl, at pH 7.4), and an appropriate amount of a peptide stock solution was added, resulting in the desired lipid to peptide molar ratio. Samples were then hydrated at 10 °C above the liquid crystalline phase of the lipids for at least 2 h, with intermittent, vigorous vortex mixing.

The large unilamellar lipid vesicles (LUVs) that were used for ITC and fluorescence experiments were prepared by the extrusion method using a Mini-Extruder (Avanti Polar Lipids Inc.). The multilamellar vesicle suspension was freeze–thawed for 5 cycles and then extruded through polycarbonate filters (0.1 μm) 13 times. The concentrations of the phospholipids were calculated on the basis of the weight of dried lipid. The peptide concentration of each of the samples was verified using the UV absorption at 280 nm and calculated molar extinction coefficients based on the number of Trp residues in each of the peptides (11,380 M^{-1} cm^{-1} for two Trps and 5650 M^{-1} cm^{-1} for one Trp).

2.3. Circular dichroism spectroscopy

CD data were acquired with a Jasco J-715 CD spectrophotometer using a 1 mm path length cylindrical cuvette. The response was measured using wavelengths from 195–255 nm with 0.2 nm step resolution and a 1 nm bandwidth. The rate was 50 nm/min and used a 2 s response time, and the spectra were averaged over 8 scans. Spectra were collected for samples of 40 μM L- and D-peptide in 10 mM Tris at pH 7 and 25 °C, with and without 50 mM SDS or DPC. For each micelle sample, a background blank of micelle was subtracted before the introduction of the peptide.

2.4. Fluorescence spectroscopy

The tryptophan fluorescence was measured using a Varian Cary Eclipse spectrophotometer. Two types of samples were prepared for analysis. One set of samples were prepared with 2 μM peptide and 130 mM NaCl in 20 mM phosphate buffer adjusted to pH 7. These samples were introduced to either 1 mM POPG or 1 mM POPC. The other set of samples was prepared using 5 mM HEPES, 5 mM MES, 5 mM citric acid, 150 mM NaCl, and 1 mM EDTA and were adjusted to pH 7. The second sets of samples were examined with lipid combinations of DOPC, DOPG, and DOPE. The concentrations were 5 μM with peptide and 150 μM lipid. For all samples, the excitation wavelength used was 295 nm and the emission scanned from 300–450 nm with a scan speed of 10 nm/s. Fluorescence quenching experiments were completed by excitation at 295 nm and monitoring the peak maximum in the absence of quenching agent, followed by increasing the concentration of acrylamide from 10 mM to 200 mM for each of the solutions studied. The effect on the peptide fluorescence by acrylamide was analyzed using the quenching constant (Ksv) as determined from the Stern-Volmer equation:

$$F_0/F = 1 + Ksv[\mathrm{Q}] \quad (1)$$

Where F_0 and F are the fluorescence intensity in the absence and presence of quencher (Q), respectively [21,22].

2.5. Isothermal titration calorimetry

ITC data were acquired using a Microcal VP-ITC calorimeter (Microcal, Norhampton, MA). Samples were prepared with 40 μM peptide and either 10 mM POPG or 10 mM POPC LUVs in 20 mM phosphate buffer with 130 mM NaCl at pH 7.4 [23]. To account for the heats of dilution, control experiments were completed by titrating lipid vesicles into a buffered solution in the absence of peptide. Each 6 μl injection was carried out over a 5 s period, with 240 s between individual injections. All experiments were carried out at 30 °C.

2.6. Differential scanning calorimetry

DSC data was collected using a Microcal high-sensitivity VP-DSC (Microcal, Norhampton, MA). MLV samples of DPPC and DPPG were prepared in 20 mM phosphate buffer with 130 mM NaCl at pH 7.4 [24]. For all samples, a heating scan rate of 60 °C/h was used. Sample runs were repeated at least twice to ensure reproducibility. Data acquisition and analysis were done using Microcal Origin software (version 5.0). The total lipid concentration used for DSC was 1.0 mg/ml. Note that DPPC and DPPG are often used for the DSC experiments, because they have a higher main phase transition temperature than PO- and DO-phospholipids do, which melt below 0 °C and can not be measured within the temperature range of the VP-DSC instrument.

2.7. NMR spectroscopy

The NMR samples were initially prepared by dissolving approximately 4 mg of peptide in H_2O:D_2O 90%:10% and adjusting the pH to 3.6–4.2 using dilute HCl or NaOH. The concentration of the peptide samples was verified using the UV absorption at 280 nm mentioned before. The micelle samples were prepared by adding approximately 200 equivalents of SDS or DPC to the peptide sample. Sodium 2,2-dimethyl-2-silapentane-5-sulfonate (DSS) was added as an internal reference.

All NMR spectra were acquired at 25°C on a Bruker Avance 500 MHz NMR spectrometer equipped with a Cryoprobe™ (Bruker Analytische Messtechnik GmbH). Two dimensional TOCSY and NOESY spectra were collected using mixing times of 150 and 120 ms, respectively. A 2D ROESY spectrum of the short peptide was acquired with a mixing time of 300 ms. All spectra were acquired with 2048×512 data points in the *F2* and *F1* dimensions using spectral widths of 6500 Hz. Water suppression for the 2D spectra was performed using the excitation sculpting technique [25]. DQF-COSY spectra with 4096×512 data points were also acquired to assist in the initial assignment of the individual residues for samples containing the IVSDGNGMNAWVAWR peptide.

2.8. Structure calculation

All NMR spectra were processed with NMRPipe and analyzed using NMRView 4.1.3 [26] on PC workstations running the Redhat (7.1) version of the Linux operating system. Spectral assignments were carried out using the method of Wüthrich [27]. For structure calculations, an iterative procedure was followed, beginning with the assignment of NOE interactions between adjacent residues. Assignment tables from NMRView were used with CNS [28] to generate initial structural conformations. These structures were used to add further unambiguous assignments and refine structures in an iterative manner until all unambiguous correlations had been assigned. The peptide structures were further refined using the program ARIA (1.1) [29–31], which calibrates the NOE distance restraints with a structure-based NOE back calculation using a relaxation matrix analysis. All ARIA runs were performed using NOE constraints from 2D NOESY data and broad dihedral constraints consistent with values suitable with the allowed Ramachandran space, along with the default parameters in the program. The agreement of the structures with the allowed Ramachandran space was verified using PROCHECK (3.4) [32,33]. In the final ARIA run, the number of structures generated in the seventh and eighth iteration was increased from 20 each to 40 and 100, respectively. The 20 lowest energy structures were retained for statistical analysis in the final iteration. Visual analysis of structures was done with the program MOLMOL (2K.1) [34].

2.9. Confocal laser-scanning microscopy

Cultures were prepared as previously described [35,36]. Briefly, single colonies of bacteria were inoculated into culture medium (3% trypticase soy broth) and cultured overnight at 37 °C. An aliquot of this culture was transferred to 50 mL of fresh medium and incubated for an additional 3 to 6 h at 37 °C to obtain the cells in midlogarithmic phase. These cells were harvested by centrifugation, washed with 10 mM sodium phosphate buffer (NAPB), pH 7.4, and resuspended in 10 ml of the same buffer. The colony forming units (cfus) per millilitre were quantified by spreading serial dilutions of the cell suspension onto three separate trypticase agar plates. Bacterial cells (10^5 cfu) in 10 mM NAPB were incubated with fluorescein-labeled peptides (25 μg/ml) at 37 °C for 30 min. After incubation, the cells were washed with 10 mM NAPB and immobilized on a glass slide. The cells were then treated briefly with 0.2% TritonX-100/NAPB. The fluorescein-labeled peptides were observed with a Carl Zeiss LSM-410 laser-scanning confocal microscope. Fluorescent images were obtained with a 488 nm bandpass filter for excitation of FITC. Software merging of images was carried out with COMOS software (Zeiss).

3. Results

3.1. NMR spectral assignment and interpretation

Initial studies began by determining the structure of the 3 peptides in the presence of micelles. Micelles are usually the most convenient method of determining high-resolution structures, as vesicles are much larger and NMR signals broaden to the point where the standard 2D experiments cannot be used [37,38].

The 2D NOESY and 2D ROESY spectra collected for the L- and D-RAWVAWR-NH_2 peptides in solution showed no indication of secondary structure. However, the 2D NOESY spectrum of L-RAWVAWR-NH_2 peptide in the presence of SDS or DPC micelles displayed numerous correlations, indicating the adoption of a preferred conformation from the interaction with the SDS micelles. The correlations had also broadened compared to the 2D NOESY spectrum of L-RAWVAWR-NH_2 in the solution without micelles, indicating that the peptide was experiencing the effects of slower tumbling as a result of the interaction with micelles. The systematic presentation of the NOE correlations is given in Fig. 2A.

The 2D NOESY spectra for the D-RAWVAWR-NH_2 peptide in the solution with DPC and with SDS gave the same correlations and nearly identical relative intensities as the spectra involving the L-RAWVAWR-NH_2 peptide. The similarity between the data sets of the 2 peptides implied that a mirror image conformation existed. Therefore, the D-peptide spectra were not used for further NMR studies.

Comparison of the α-proton chemical shifts with CSI values [39] favoured coiled character for the backbone residues Trp3–Arg7 (see Fig. 2A and B). The interaction of the peptide with the neutral detergent (DPC) indicated that electrostatic forces were not the only cause of the interaction of the peptide with the micelle.

The three NOESY spectra acquired for the peptide IVSDGNGMNAWVAWR-NH_2 (with and without micelles) all displayed a second set of much weaker correlations for protons of the N-terminal residues (Ile1–Asn6). Since

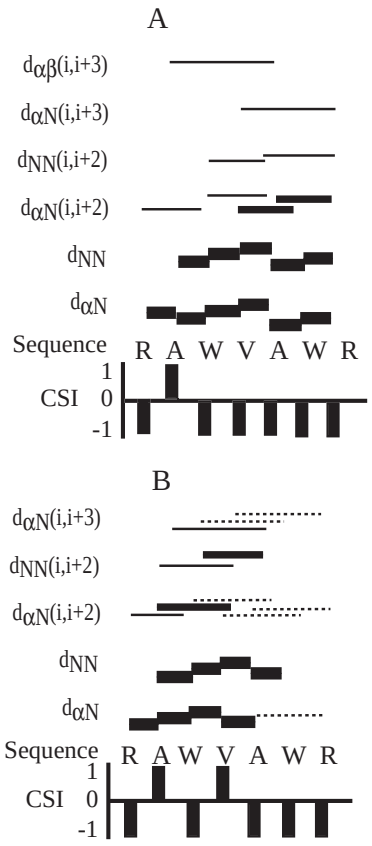

Fig. 2. ^{1}H NMR summary indicating the interactions observed in the 2D NOESY spectra for the L-peptide with (A) SDS and (B) DPC. The thickness of the lines (strong, medium, and weak) indicates the intensity of the observed NOE interactions. Dashed lines indicate ambiguous NOEs. Data are summarized from final data report from Aria. The CSI is indicated for the alpha protons below the sequence.

HPLC chromatograms and mass spectra indicated that the peptide was pure (data not shown), these peaks were attributed to a minor conformation and not further analysed.

In contrast to the short peptide, the 2D NOESY spectra of the long peptide with and without DPC or SDS micelles showed a significant number of backbone amide proton to side chain inter-residue interactions pointing to defined secondary structure in the solution. The proton–proton interactions from the 2D NOESY spectra are shown in Fig. 3. The CSI values for the long peptide with and without detergent also support the tendency toward helical character for the backbone section Gly7–Arg15 (see Fig. 3). The adoption of a helical shape for the C-terminal portion of the peptide in the aqueous solution reflected the intrinsic propensity of this sequence to form a helical conformation in human and chicken lysozyme (Gly104–Arg112) (code 1LZS and 1HEW in the Protein Data Bank).

Further examination of the N-terminal correlations for both conformations of the long peptide also indicated that there were very few inter-residue interactions when compared to the C-terminal end. This observation implied a larger degree of conformational flexibility for the N-terminal end as compared to the C-terminal residues. The variability in α-proton frequencies evaluated using the chemical shift index for the N-terminal portion of the peptide, as shown in Fig. 3, also suggested that a well-defined conformation is not present in this region.

3.2. Structural calculations

The qualitative data presented by the NMR spectra were further exploited by using proton nuclear Overhauser interactions to give more precise structural information. After the identification of the peaks in the ^{1}H NMR spectra, the intensity of the correlations in the 2D NOESY spectra was used to provide distance constraints for structural calculations. After assigning all peak intensities, a complete list of unambiguous and ambiguous assignments was submitted for final structural determination using Aria. The program Aria uses a rigorous simulated annealing protocol to reduce the energy of generated structures to low levels while maintaining conformity with assigned constraints [29–31,40].

Structural statistics obtained for the short peptide L-RAWVAWR-NH_2 in SDS and DPC are presented in Table 1. Approximately 20 restraints per amino acid were used in both types of micelles. Examination of the structures in MOLMOL indicates a coiled peptide backbone for Val4–Arg7, with a preceding bend for Ala2–Trp3 for the peptide with both SDS and DPC (see Fig. 4). A comparison of the 2 sets of 20 lowest energy structures for both SDS and DPC indicated that the rmsd value of the backbone atoms for both systems combined was 0.718 Å. This value increased to 1.884 Å when the heavy side chain atoms were included.

Similar to other reports of peptides interacting with lipids where the aromatic rings of Trp residues are arranged on the same side of the peptide backbone [41], the indole rings in the short peptide are oriented to allow simultaneous interaction with a lipid surface. Further examination of the structure indicated that the charged termini of the arginine side chains point in the same direction in the structure. Without a longer peptide chain, the energetically favoured formation of a regular coil in the short peptide may be in competition with the electrostatic interactions between the peptide and the membrane that anchor the terminal arginine side chains. As a result, the peptide may be simply too short for a regular helix to be energetically favoured.

The correlations for the longer peptide under the three types of conditions indicated that the N-terminal portion of the peptide displayed fewer inter-peptide NOE interactions than the C-terminal end. Fewer distance constraints in the N-terminal region result in a poor rmsd agreement for the backbone and side chain heavy atom comparison for the entire peptide (Table 2). However, the conformational overlap of the 20 lowest energy conformations improves dramatically when only the C-terminal portion (Gly7–

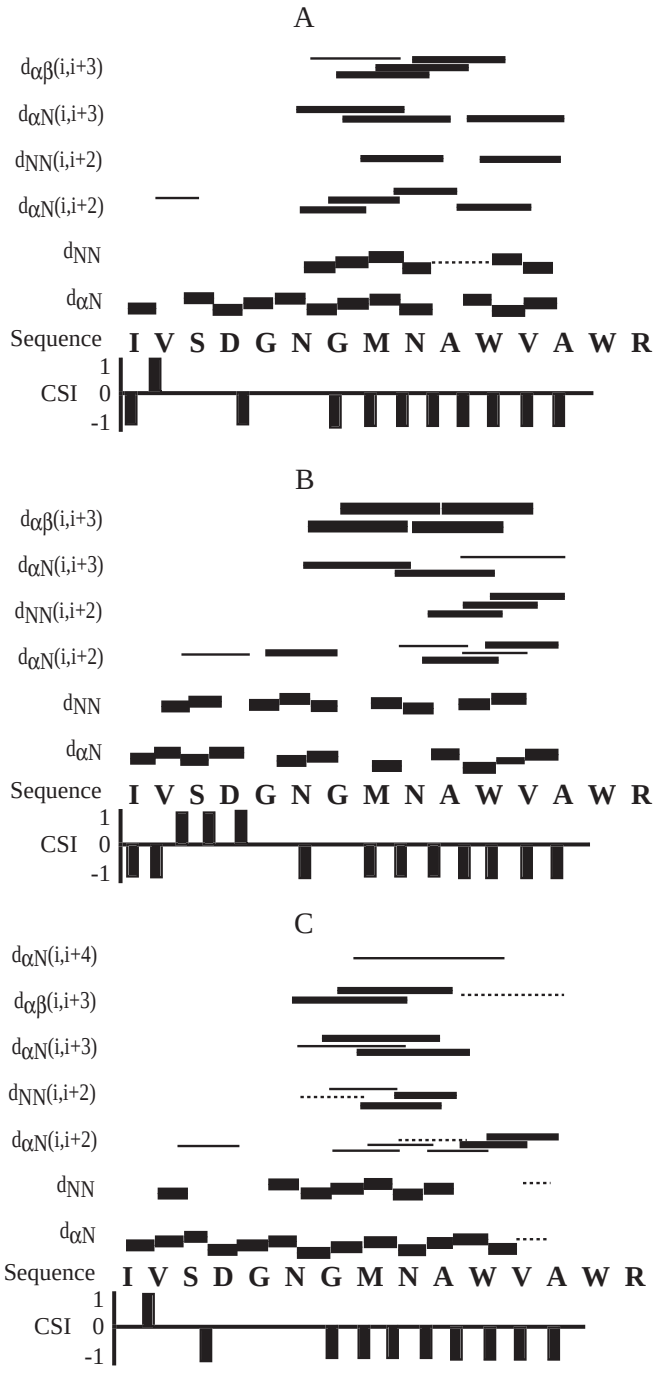

Fig. 3. ^{1}H NMR summary indicating the interactions observed in the 2D NOESY spectra for the long peptide (A) without micelles, (B) with SDS, and (C) with DPC. The thickness of the lines (strong, medium, and weak) indicates the intensity of the observed NOE interactions. Dashed lines indicate ambiguous NOEs. Data are summarized from final data report from Aria. The CSI is indicated for the alpha protons below the sequence.

Arg15) is compared. For the long peptide without micelles, as well as with SDS and DPC, the backbone and heavy atom rmsd for the C-terminal region becomes less than 1 Å in all cases.

A visual inspection of the conformations obtained from the structural calculations using MOLMOL indicated a few interesting features. As expected, the lack of constraints for the N-terminal portion of each peptide (Ile1–Asn6) produced a random coil structure for the combined 20 lowest energy structures. All 3 structures show that both Trp aromatic rings are on the same side of the peptide in each case, albeit with different mutual orientations.

In each case, the structures indicated that the long peptide had various degrees of helical conformation in the C-terminal portion (Gyl7–Arg15) of the sequence. For the long peptide in solution without micelles, the helical portion involved Gly7–Trp11, followed by a bend in the

Table 1
Structural statistics for the final 20 structures of short L-peptide with SDS and DPC

	SDS	DPC
Number of distance restraints		
Unambiguous NOEs	157	161
Ambiguous NOEs	1	14
Unassigned NOEs	0	0
Total NOEs	158	175
Number of broad dihedral restraints	6	6
rms Distances from ideal values		
Bonds (Å)	2.08×10^{-3}	$1.74\times10^{-3}\pm1.52\times10^{-4}$
Angles (degree)	$0.40\pm1.09\times10^{-2}$	$0.33\pm1.52\times10^{-2}$
Impropers (degree)	$0.18\pm1.90\times10^{-2}$	$0.18\pm1.90\times10^{-2}$
van der Waals (kcal/mol)	6.35±0.79	8.07±0.67
Distance restraints		
Unambiguous (Å)	$1.15\times10^{-2}\pm4.11\times10^{-3}$	$5.89\times10^{-2}\pm4.45\times10^{-2}$
Ambiguous (Å)	–	$1.65\times10^{-3}\pm7.20\times10^{-3}$
All distance restraints (Å)	$1.14\times10^{-2}\pm4.10\times10^{-3}$	$5.67\times10^{-2}\pm4.28\times10^{-2}$
Dihedral restraints (degree)	0.65±0.20	0.30±0.25
Non-bonded energies		
Electronic (kcal/mol)	−94.69±23.24	−90.99±24.32
van der Waals (kcal/mol)	−52.88±12.16	−48.88±11.31
Ramachandran (%)[a]		
Most favoured	40	25
Additionally allowed	60	59
Generously allowed	0.0	16
Disallowed	0.0	0.0
Global rms distance (Å)[b]		
Backbone	0.236	0.332
Heavy	0.870	0.869

[a] As determined by PROCHECK.
[b] Calculated using MOLMOL.

coil for Val12–Arg15. The long peptide with SDS micelles displayed a helical segment from Trp11–Trp14, preceded by a bend in the coil from Met8–Ala10. Yet, the appropriate constraints were available to form a complete helix for Met8–Trp14 of the long peptide in DPC micelles.

A search of each set of 20 structures revealed that the correct geometry existed in all of the 5 structured peptides (2 RAWVAWR-NH_2 and 3 long peptides) to suggest the possibility of intra-residue hydrogen bonds near the C-terminal end of the peptides. The formation of the hydrogen bonds would lower the energy of the structure, perhaps by 0.3–0.7 kcal mol^{-1} per residue [42].

3.3. CD spectroscopy

Circular dichroism provided another valuable method of comparing the differences in structure for the 3 peptides in the presence of micelles. The CD spectra collected for the L-RAWVAWR-NH_2 peptide in solution are shown in Fig. 5. Upon combining the L-peptide and micelles, the negative molar ellipticity, suggestive of a coiled shape, changed to a recognizable positive value, indicative of helical character in the region of 185–195 nm. The region from 195 to 225 nm also retained the characteristic shape expected for a coiled or helical peptide. There was some variability in this region consistent with subtle differences expected for a short 7 residue peptide.

Fig. 5 also shows a comparison of CD spectra for both the L- and D-RAWVAWR-NH_2 peptides with SDS micelles. The symmetry of both spectra about a horizontal axis suggests that the conformations adopted by the L- and D-peptides are mirror images of each other when interacting

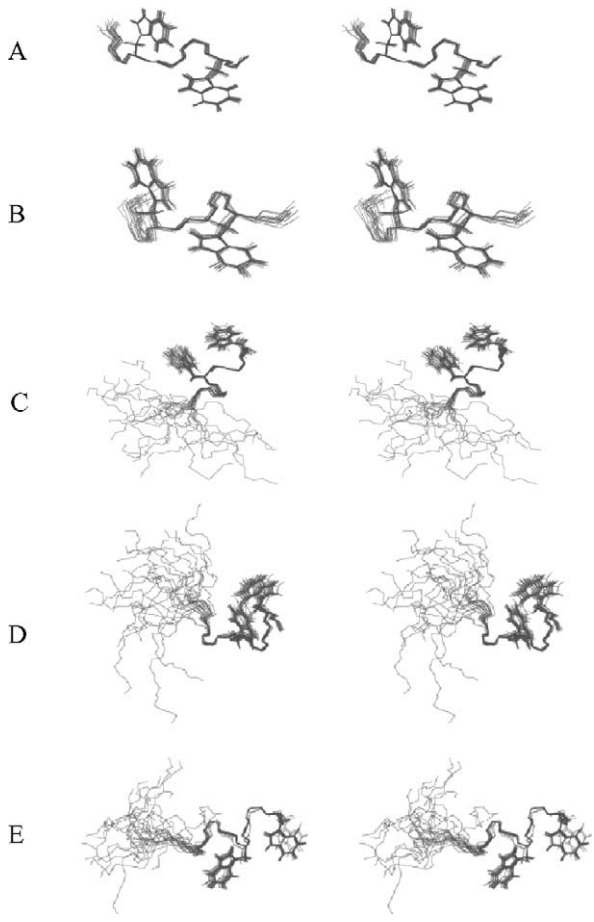

Fig. 4. Single representation cartoon structures (left) and stereo-diagrams of the backbone trace of the 20 lowest energy structures (right) of: (A) short peptide with SDS, (B) short peptide with DPC, (C) long peptide without micelles, (D) long peptide with SDS, and (E) long peptide with DPC. Panels (A) and (B) were generated by fitting all of the backbone atoms. Panels (C)–(E) were generated by fitting the backbone atoms for residues Met8–Arg15. This figure was generated with the program MOLMOL.

Table 2
Structural statistics for the final 20 structures of the long peptide: without micelles, with SDS and DPC

	Peptide	SDS	DPC
Number of distance restraints			
Unambiguous NOEs	148	199	239
Ambiguous NOEs	2	2	15
Unassigned NOEs	0	0	0
Total NOEs	150	201	154
Number of broad dihedral restraints	12	12	12
rms Distances from ideal values			
Bonds (Å)	1.18×10^{-3}	$1.38\times10^{-3}\pm1.07\times10^{-4}$	$1.53\times10^{-3}\pm1.50\times10^{-4}$
Angles (degree)	$0.23\pm1.13\times10^{-2}$	$0.24\pm1.37\times10^{-2}$	$0.31\pm1.62\times10^{-2}$
Impropers (degree)	$0.17\pm1.94\times10^{-2}$	$0.17\pm2.22\times10^{-2}$	$0.23\pm2.89\times10^{-2}$
van der Waals (kcal/mol)	7.13±0.61	7.23±1.10	8.93±0.96
Distance restraints			
Unambiguous (Å)	$6.39\times10^{-3}\pm1.30\times10^{-2}$	$3.20\times10^{-2}\pm2.54\times10^{-2}$	$2.47\times10^{-2}\pm2.31\times10^{-2}$
Ambiguous (Å)	–	$1.33\times10^{-3}\pm4.20\times10^{-3}$	
All distance restraints (Å)	$6.35\times10^{-3}\pm1.29\times10^{-2}$	$3.17\times10^{-2}\pm2.52\times10^{-2}$	$2.40\times10^{-2}\pm2.23\times10^{-2}$
Dihedral restraints (degree)	–	$5.09\times10^{-2}\pm0.10$	$1.94\times10^{-2}\pm4.22\times10^{-2}$
Non-bonded energies			
Electronic (kcal/mol)	−372.66±89.13	−388.27±92.80	−391.62±92.44
van der Waals (kcal/mol)	−77.33±17.92	−78.58±18.22	−85.96±19.85
Ramachandran (%)[a]			
Most favoured	83.6	64.5	82.7
Additionally allowed	16.4	35.5	17.3
Generously allowed	0.0	0.0	0.0
Disallowed	0.0	0.0	0.0
Global rms distance (Å)[b]			
Backbone	2.467	2.306	2.346
Heavy	3.595	2.790	2.847
Gly7–Arg15			
Backbone	0.373	0.365	0.287
Heavy	0.987	0.640	0.644

[a] As determined by PROCHECK.
[b] Calculated using MOLMOL.

with the micelle. This result is consistent with all of the NMR data indicating that the change in pH from neutral (CD) to acidic (NMR) conditions does not have a noticeable effect upon the coiled conformation of the short peptides.

The CD spectra for the long peptide indicate that a combination of helical and random coil content dominate the spectra. The long peptide shows a large proportion of random coil, with a minimum at 198 nm. The introduction of DPC shifted the spectra to a double minimum at 204 and 217 nm and a more positive elipticity at 195 nm. The peptide in SDS developed a large positive elipticity at 195 nm but shows only a single pronounced minimum at 207 nm. Together, the CD spectra of the long peptide established that variable amounts of coiled character exist in the presence of the two detergents.

3.4. Fluorescence spectroscopy

Data acquired from tryptophan fluorescence studies can be used to gain qualitative insight into the environment of the fluorophores upon interaction with lipids. The fluorescent properties of the Trp indole rings of the L-RAWVAWR-NH_2 peptide were studied using both uniform and mixed lipid vesicle systems. Negatively charged POPG vesicles were used to mimic bacterial membranes and POPC was used to resemble zwitterionic eukaryotic membranes [9,43]. The fluorescence emission spectra of the L-peptide with POPC and POPG vesicles are shown in Fig. 6. In the aqueous solution, the short peptide exhibited an emission maximum at 355 nm, similar to a Trp control sample. The binding of the L-RAWVAWR-NH_2 peptide to the various lipids caused blue shifts in the emission maximum of 12 nm for POPG, while the emission maximum of the peptide in the presence of POPC remained essentially unchanged. Each of these shifts was accompanied by an increase in fluorescence intensity, consistent with the partitioning of the Trp side chain into a more hydrophobic, sterically confined environment [22]. The values of the emission maxima were the same for both the L- and D-peptides, while the long peptide

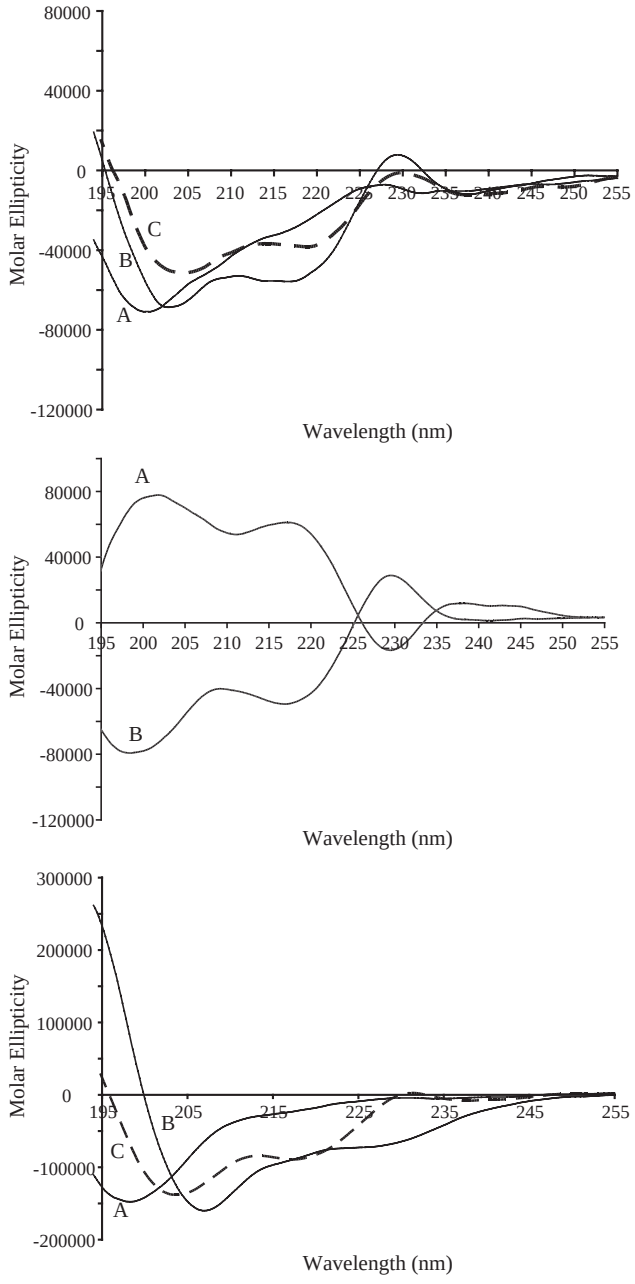

Fig. 5. Top: CD spectra of 40 mM short L-peptide at 25 °C in 10 μM Tris (pH 7.0): (A) without micelles, (B) with 50 mM SDS, and (C) with 50 mM DPC. Centre: CD spectra of 50 mM SDS at 25 °C in 10 μM Tris (pH 7.0): (A) with 40 μM short D-peptide and (B) with 40 μM short L-peptide. Bottom: CD spectra of 40 mM long peptide at 25 °C in 10 μM Tris (pH 7.0): (A) without micelles, (B) with 50 mM SDS, and (C) with 50 mM DPC.

maintained the same value of 356 nm for each of the solutions tested.

To determine the degree of interaction of the Trp side groups with the lipids, fluorescence quenching experiments were performed using acrylamide. In phosphate buffer, the Stern-Volmer constants (Ksv) for the 2 short peptides are shown in Table 3. The interaction of the aromatic rings with the quenching reagent becomes

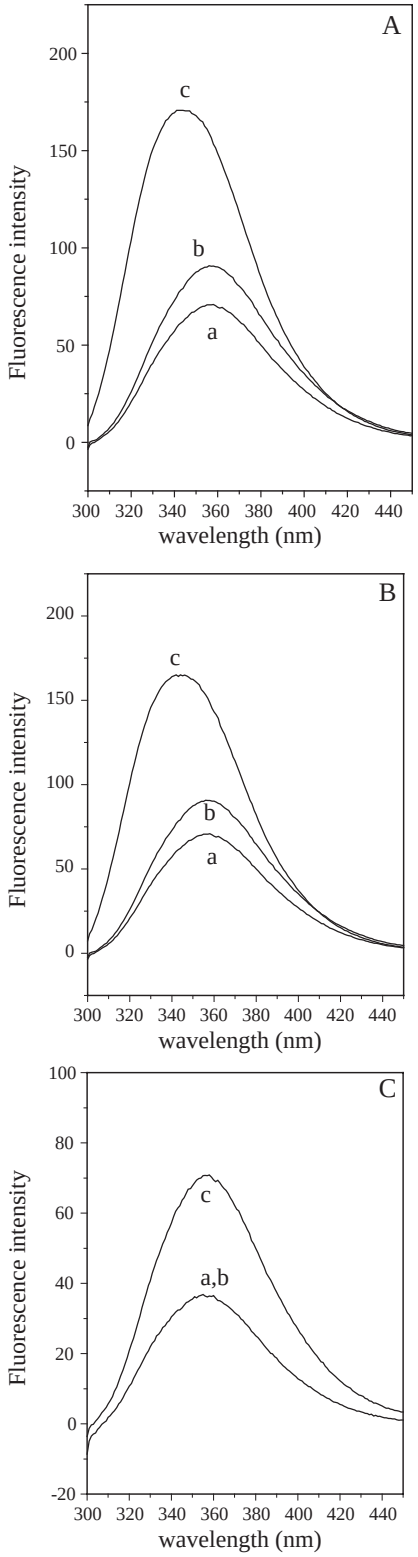

Fig. 6. Fluorescence emission spectra of: (A) 5 μM L-peptide, (B) 5 μM D-peptide, and (C) 2 μM long peptide in 20 mM phosphate buffer with 130 mM NaCl adjusted to pH 7. The curves represent (a) buffer only, (b) 1 mM POPC, and (c) 1 mM POPG.

Table 3
Stern-Volmer constants (M^{-1}) for acrylamide quenching experiments between peptides and lipid vesicles

Peptide type	Peptide only[a]	POPG[a,b]	POPC[a,b]	Peptide only[c]	DOPE:DOPG[c,d] (6:4)	DOPC:DOPG[c,d] (6:4)	DOPC:DOPE[c,d] (1:1)
L-	21.0	1.9	17.5	18.43 (1.44)	6.20 (0.54)	6.59 (0.59)	15.25 (0.37)
D-	20.5	2.2	16.8	16.49 (0.438)	6.20 (0.57)	6.98 (0.38)	14.69 (0.73)
Long	–	–	–	16.24 (0.99)	15.04 (0.50)	14.13 (2.39)	15.06 (0.46)

Values are the average of 3 separate experiments. Standard deviation values are indicated in brackets.
[a] Samples were prepared with 2 μM peptide in 20 mM phosphate buffer with 130 mM NaCl at pH 7.4.
[b] Lipid concentration was 1 mM.
[c] Samples were prepared in 5 μM peptide, 5 mM HEPES, 5 mM MES, 5 mM citric acid, 150 mM NaCl and 1 mM EDTA and adjusted to pH 7.
[d] Lipid concentration was 7.5 mg/ml.

less pronounced as the Trp indole rings interacted less with the acrylamide quenching agent. Further study of Stern-Volmer constants indicated that the next strongest interaction with the quenching agent is seen with neutral surface of the series: POPC and DOPC:DOPE 1:1. The next strongest interaction with acrylamide is DOPC:-DOPG, DOPE:DOPG, and POPG lipid. The similarity in interaction of the long peptide in each of the 3 mixed systems indicated an indifference of the long peptide for interaction with the lipid interface. In addition, results obtained with PO- and DO-phospholipids were comparable, even though PO have a relatively high main phase transition temperature; nevertheless, both are below room temperature where the measurements are made.

3.5. Differential scanning calorimetry

DSC is a very sensitive method of studying the changes in the thermotropic phase transition of the widely studied MLVs DPPC and DPPG [44–46]. The DSC heating thermograms obtained from the interaction of DPPG or DPPC vesicles in the absence and presence of the 3 peptides are shown in Fig. 7. The interaction of the long peptide and the negatively charged DPPG vesicles is indicated in Fig. 7A at a lipid:peptide ratio of 10:1. Even at this high concentration of peptide, there is little or no effect upon the main transition from gel to liquid crystalline phase at 40.5 °C.

The interaction of L-RAWVAWR-NH_2 peptide at different lipid-to-peptide molar ratios is presented in Fig. 7B. The thermograms indicate that the addition of the L-RAWVAWR-NH_2 peptide had a small but consistent effect on the phase behaviour of DPPG vesicles. The pretransition from the lamellar- $L_{\beta'}$ gel to the lamellar ripple phase of pure DPPG at 33 °C and its main transition from the gel to the liquid crystalline L_α phase at 40.5 °C are consistent with previously published data [47]. At high molar ratios of lipid to peptide, little effect on the main phase transition was observed, although visible differences in the pretransition were detected. With increasing amounts of peptide, the pretransition was less pronounced until it disappeared at the lipid:peptide ratio of 25:1. Any further increase of the amount of peptide resulted in the introduction of a two-component main transition at a lipid:peptide ratio of 15:1. This progression of main transition complexity is consistent with the separation of the lipid surface into domains either rich in peptide or peptide deficient. Enthalpies calculated for the entire transition range (Table 4) are comparable to the value of pure DPPG even though the phase behaviour of DPPG vesicles was influenced by the addition of the L-RAWVAWR-NH_2 peptide. Peptides or proteins interacting with the hydrophobic interior regions of membranes often exhibit a large reduction in the transition enthalpy. Therefore, these results suggest that the L-RAWVAWR-NH_2 peptide does not penetrate deeply into the hydrophobic region of DPPG vesicles and most likely resides at the solvent–lipid interface.

The results of the DSC experiments with the D-RAWVAWR-NH_2 peptide mirrored those of the L-peptide, indicating again that chiral recognition does not play a role in the membrane binding of this peptide (Fig. 7C). DSC heating thermograms illustrating the effect of the L- and D-RAWVAWR-NH_2 peptide on the thermotropic phase behaviour of DPPC vesicles are presented in Fig. 7D. Aqueous dispersions of DPPC also exhibited a pretransition at 35.2 °C and a main phase transition at 41.4 °C [44]. In contrast to DPPG, the addition of L- or D-peptide had no effect on the phase behaviour of DPPC even at a low lipid to peptide ratio of 10:1. This result emphasizes the stronger interaction of the L- or D-peptide with negatively charged DPPG while having very little effect on the neutral DPPC.

3.6. Isothermal scanning calorimetry

The use of ITC provided an opportunity to determine whether the difference in interactions between neutral and negative lipids would be detectable and reflected by titration calorimetry [23,48,49].

The enthalpy of binding was studied by titrating either POPC or POPG vesicles into each of the 3 peptides. By subtracting the control experiments used to determine the heat of dilution and correcting for the molar amount of injected peptide, the molar enthalpy of binding (ΔH) was obtained. Results of the interaction of

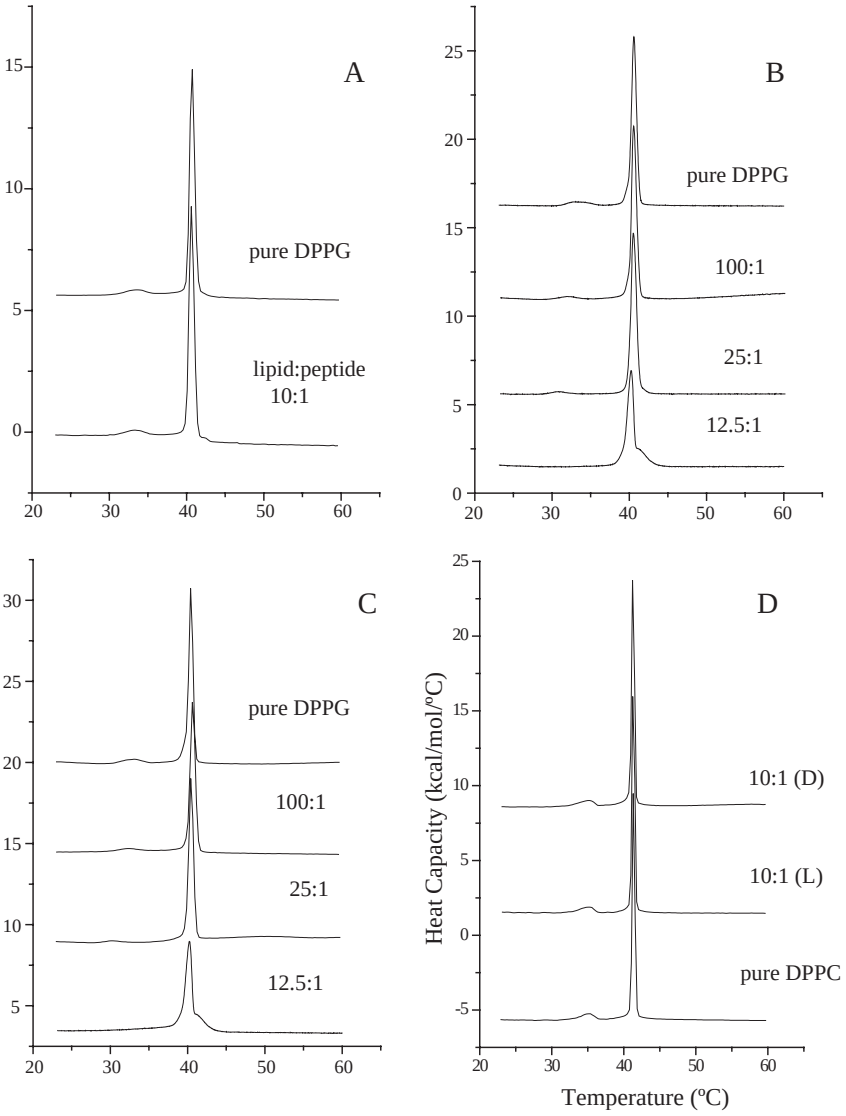

Fig. 7. DSC heating scans of: (A) pure DPPG and DPPG:long peptide at a molar ratio of 10:1; (B) DPPG and various lipid:L-peptide molar ratios; (C) DPPG and various lipid:D-peptide molar ratios; and (D) DSC heating scan of DPPC and various lipid:short peptides molar ratios. All samples were in the 20 mM phosphate buffer at pH 7.4.

the long peptide to either POPC or POPG indicated that the energy change was below the sensitivity limit of the technique. The result was the same for samples of the L- or D-RAWVAWR-NH_2 peptides with the neutral vesicle POPC. The binding of both the L- and D-RAWVAWR-NH_2 peptides to POPG are shown in Fig. 8.

Table 4
Thermodynamic parameters determined by DSC for the interaction of L-RAWVAWR-NH_2 with the lipid bilayers

	ΔH_{pre} (kcal/mol)	T_{pre} (°C)	T_{domain} (°C)	ΔH_{domain} (kcal/mol)	T_{main} (°C)	ΔH_{main} (kcal/mol)
Pure DPPG	0.73	33.55	–	–	40.61	8.56
100:1[a]	0.34	31.99	–	–	40.47	8.85
25:1	0.32	30.80	–	–	40.42	8.90
15:1	0.17	31.20	42.04	0.62	40.27	7.52
12.5:1	–	–	41.75	1.59	40.17	6.55
Pure DPPC	1.45	35.45	–	–	41.42	9.32
100:1	1.45	35.45	–	–	41.42	9.32
12.5:1	1.45	35.45	–	–	41.42	9.32

pre=pretransition.
main=main phase transition.
[a] Ratio of lipid:peptide.

The binding enthalpies and binding constants calculated from this data are the same within experimental error, indicating that peptide insertion is an exothermic process

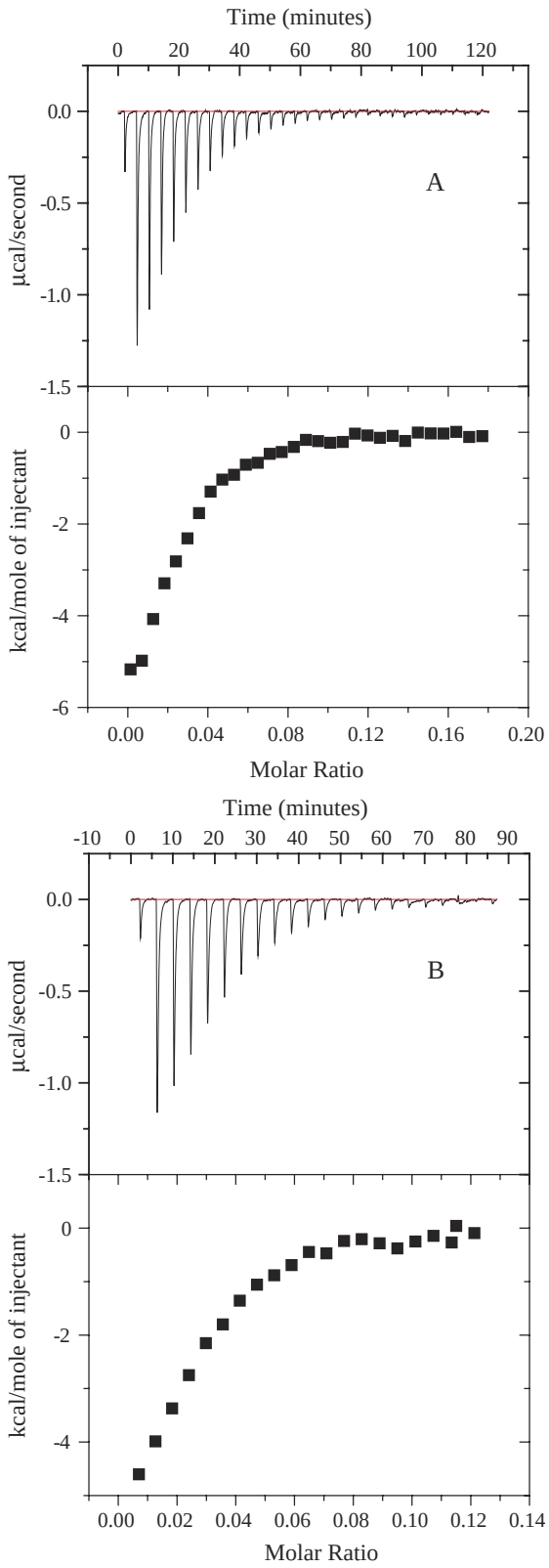

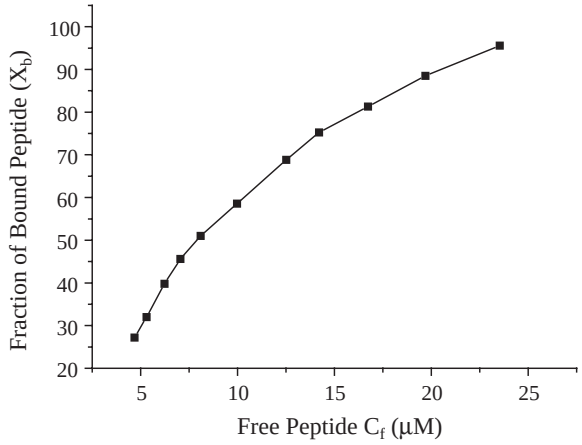

Fig. 9. Binding isotherms of RAWVAWR-NH_2 with POPG. C_f is the equilibrium concentration of the free peptide in solution. X_b is the molar ratio of the bound peptide per lipid (mmol/mol).

with a very large binding constant. Again, the trends shown by the other analyses are reflected by ITC and suggest the L- and D-RAWVAWR-NH_2 peptides bind in the same manner to the negatively charged POPG LUVs.

Additional information regarding organization of the peptide after binding to the lipid can be obtained from the ITC data. Analysis of the binding isotherm of the L-peptide with POPG is shown in Fig. 9. The gradual decrease in the slope of the curve is suggestive of a simple adhesion process in a non-cooperative manner that does not involve the aggregation of the peptide on the lipid surface [50].

3.7. Confocal laser-scanning microscopy

The lack of strong interaction with the membrane mimetic systems caused us to probe whether the RAW-VAWR-NH_2 peptide was able to penetrate actual bacterial membranes. The images shown in Fig. 10 clearly indicate the ability of the fluorescein labeled peptide (at a concentration of 25 µg/ml) to readily penetrate the membranes and accumulate in the cytoplasm of both *E. coli* and *S. aureus*. The strong intensity over the confocal microscope image of each bacterium indicates the location of the labeled peptide in the cytoplasm. Had the peptide been associated with mostly the membrane region, the intensity would have been greatest in a halo representing

Fig. 8. Titration calorimetry of: (A) short L-peptide and (B) short D-peptide with POPG lipid vesicles. The lower curve in each case represents the heat of reaction as a function of injection number as measured by peak integration. Using a one site model, the statistics are χ^2=61.77, reaction stoichiometry=0.1798±0.0079, binding constant=5.086×10^4±6353, ΔH=−4210±78.58, and ΔS=7.644 for Panel (A) and χ^2=22.14, reaction stoichiometry=0.1650±0.0042, binding constant=5.378×10^4±4121, ΔH=−4211±48.86, and ΔS=7.755 for Panel (B).

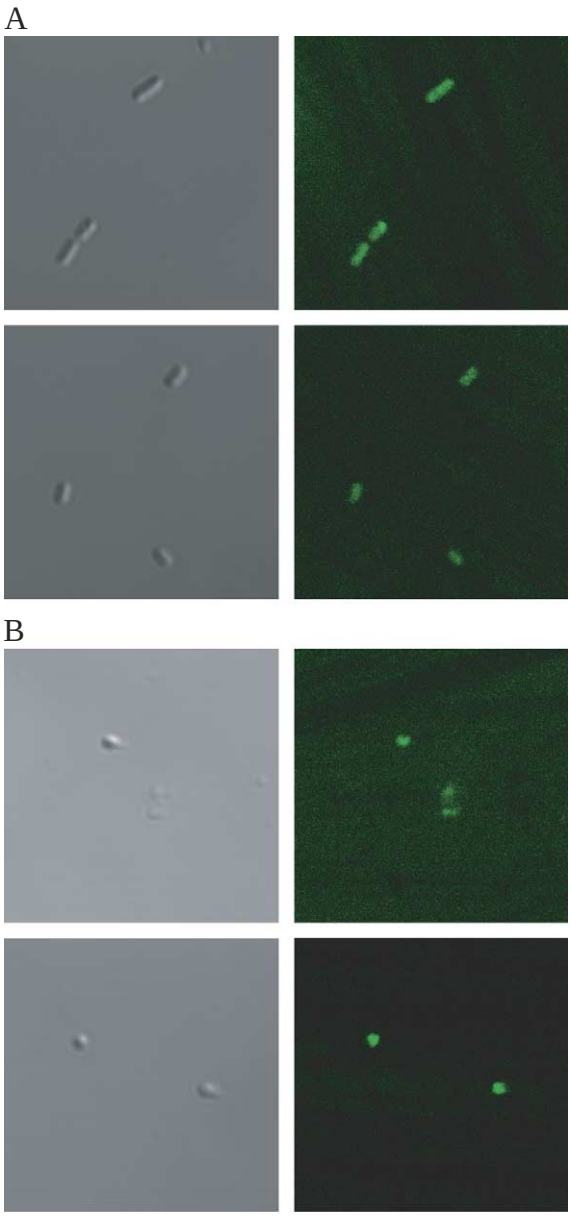

Fig. 10. Images of fluorescein labeled RAWVAWR-NH_2 from light microscope (left) and confocal microscope (right) in *E. coli* (A) and *S. aureus* (B). The even intensity across the entire area of the bacteria indicates peptide in the cytoplasm.

the membrane region [36] and weaker over the centre of each bacterium.

4. Discussion

The variety of techniques used in this study provides a comprehensive method for comparing the binding of three related antimicrobial peptides to both bacterial and eukaryotic membrane mimetic systems. Clearly, the complimentary nature of the data supplied by each technique provides unique insight into the peptide interactions with these model membrane systems. For both the short (L-RAWVAWR-NH_2) and long (IVSDGNGMNAWVAWR-NH_2) peptides, the extent of interaction with model bacterial and eukaryotic membranes reflected the difference in antimicrobial activity found in the previous study [10]. Together, fluorescence, DSC and ITC results all indicate a very weak interaction between the long peptide and any of the detergent or lipid systems. Data from NMR, however, suggest that interaction between the long peptide and detergent is subtle and only induces slight change in the conformation of the peptide. From this comparison, a relative order of sensitivity of the various techniques is evident, with NMR being the most sensitive to monitor subtle conformational changes.

Collectively, the data suggest that the ability of the AWVAWR portions of both the long and short peptides to develop coiled or helical shape is not sufficient to induce antimicrobial activity. This portion in both the short and long peptide in this same region also formed helical structure in the intact lysozyme protein. The ability to form a helical shape has been calculated to reduce the free energy of the system by 0.4 kcal mol^{-1} per residue in melittin [42] and 0.14 kcal mol^{-1} in magainin-2 amide [51]. Yet, the short peptide forms a preferred coiled character on the surface of both neutral and negative lipids, suggesting that the insertion of the side chain groups is responsible for the exothermic properties and not the tendency of the backbone to form a regular structure. The additional cationic group provided by changing Asn to Arg may supply the electrostatic charge necessary to enhance binding with a negatively charged lipid surface. Indeed, a minimum of two Arg residues seems to be required to generate the observed antimicrobial effect [9,10]. The formation of a helical conformation for Gly7–Arg15 did not confer tighter binding of the long peptide to DPC. Contrary to previous suggestions, the formation of a coiled structure in these peptides is not sufficient to confer antimicrobial properties [13].

Our work indicates that there is no appreciable difference between the L- and D-RAWVAWR-NH_2 peptides with respect to interactions with lipid model membranes. Any difference in activity in the all L- and all D-peptide would suggest that chiral recognition sites (receptors or perhaps intracellular RNA, DNA, or enzymes) are involved with these peptides as have been suggested in other studies [6,7,52]. Recent work has shown that RNA and DNA synthesis is inhibited shortly following the addition of the short peptides to microbes, supporting that the latter may be an important intracellular site of activity for these peptides [14].

Including DSC data, the information supports the notion that peptides affect lipid packing in membranes (see Fig. 7). On a larger scale, the ITC results indicate a non-cooperative interaction of the L-peptide with the PG lipid, indicating that a random distribution of peptides takes place on the surface of the vesicle. Therefore, at sufficient peptide concentration, any membrane disruption might occur in a mechanism consistent with the proposed carpet-like formation [53].

Although this peptide binds tightly to the negatively charged or mixed membrane mimetic systems, the peptide

initially resides if not at the surface, then in the interface region. It is well known that the outer leaflets of bacterial and eukaryotic cell membranes have a markedly different composition. The latter are comprised mostly of the zwitterionic PC headgroups, while the bacterial cytoplasmic membrane is a mixture of zwitterionic PE and negatively charged PG [43]. It would appear that the cationic peptides studied here bind strongly to the interface of a bacterial membrane and not the hydrophobic side chain. Since these peptides are too short to span the membrane and form channels, their antimicrobial activity arises from the ability to either immediately alter the membrane characteristics and/or traverse the membrane spontaneously and act as intracellular targets. The former possibility would seem to occur only as a means of entering the cell since calcein leakage assays with RAWVAWR-NH_2 have shown that under conditions where other antimicrobial peptides disrupt vesicles, RAWVAWR-NH_2 does not cause calcein leakage from vesicles (unpublished results). Several studies support the notion that Arg rich peptides, similar to the ones studies here, can spontaneously cross membranes [9,54]. Indeed, proposed rapid passage of RAWVAWR-NH_2 across the bacterial membrane may proceed in an analogous fashion to the cationic Arg-rich antimicrobial peptide buforin II [35,36] or PR-39 [55], which enters and kills the cell without causing membrane leakage. Thus, previously noted increased permeability of the outer and inner bacterial membranes [14] of *E. coli* after the introduction of lysozyme peptides would not appear to arise from direct action of the peptides with the phospholipids but instead may be caused by the interaction of other non-lipid membrane sites and/or the dissipation of membrane potential [13]. Since the confocal microscopy studies indicated that fluorescein labeled peptide collected quickly in the cytoplasm of both *E. coli* and *S. aureus*, it is most likely that the difference in binding properties of the peptides with model membrane systems determines the relative ability or rate that the peptides are able to transfer to the interior of the cell.

Therefore, our results suggest that these antimicrobial peptides interact with the phospholipids present in the bacterial membrane primarily as a means of promoting internalization of the peptides in order to affect intracellular functions. This explains how the L- and D- short peptides can have a different physiological activity, while interacting in the same manner with the membrane. Future work with this system would involve specifically identifying the targets that cause the reported difference in antimicrobial activity between the L- and D-peptides.

Acknowledgements

The authors would like to thank the Canadian Foundation for Innovation (CFI), the Alberta Science and Research Authority (ASRA), the Alberta Intellectual Infrastructure and Partnership Program (IIPP), and AHFMR for the financial support in purchasing the Cryo-probe and upgrades to the 500 MHz NMR console for the Bio-NMR facility. In addition, the Bio-NMR facility is supported by a maintenance grant from Canadian Institutes for Health Research. The DSC, ITC, and Fluorescence spectrophotometer were purchased with funds from ASRA and the Western Economic Development (WED) foundation provided to the Alberta Network for Proteomics Innovation. The CD spectrophotometer was purchased by the Department of Chemistry at the University of Calgary with funding from the Natural Sciences and Engineering Research Council of Canada.

References

[1] S.A. Muhle, J.P. Tam, Design of Gram-negative selective antimicrobial peptides, Biochemistry 40 (2001) 5777–5785.
[2] K. Matsuzaki, Why and how are peptide–lipid interactions utilized for self-defense? Magainins and tachyplesins as archetypes, Biochim. Biophys. Acta 1462 (1999) 1–10.
[3] J.P. Tam, Y.A. Lu, J.L. Yang, Design of salt-insensitive glycine-rich antimicrobial peptides with cyclic tricystine structures, Biochemistry 39 (2000) 7159–7169.
[4] W.T. Heller, A.J. Waring, R.I. Lehrer, T.A. Harroun, T.M. Weiss, L. Yang, H.W. Huang, Membrane thinning effect of the beta-sheet antimicrobial protegrin, Biochemistry 39 (2000) 139–145.
[5] H.W. Huang, Action of antimicrobial peptides: two-state model, Biochemistry 39 (2000) 8347–8352.
[6] R.M. Epand, H.J. Vogel, Diversity of antimicrobial peptides and their mechanisms of action, Biochim. Biophys. Acta 1462 (1999) 11–28.
[7] P.M. Hwang, H.J. Vogel, Structure–function relationships of antimicrobial peptides, Biochem. Cell. Biol. 76 (1998) 235–246.
[8] A.M. Cole, T. Ganz, Human antimicrobial peptides: analysis and application, BioTechniques 29 (2000) 822–831.
[9] H.J. Vogel, D.J. Schibli, W. Jing, E.M. Lohmeier-Vogel, R.F. Epand, R.M. Epand, Towards a structure-function analysis of bovine lactoferricin and related tryptophan- and arginine-containing peptides, Biochem. Cell. Biol. 80 (2002) 49–63.
[10] A. Pellegrini, U. Thomas, N. Bramaz, S. Klauser, P. Hunziker, R. von Fellenberg, Identification and isolation of a bactericidal domain in chicken egg white lysozyme, J. Appl. Microbiol. 82 (1997) 372–378.
[11] C.A. Parish, H. Jiang, Y. Tokiwa, N. Berova, K. Nakanishi, D. McCabe, W. Zuckerman, M.M. Xia, J.E. Gabay, Broad-spectrum antimicrobial activity of hemoglobin, Bioorg. Med. Chem. 9 (2001) 377–382.
[12] W.M. Shafer, F. Hubalek, M. Huang, J. Pohl, Bactericidal activity of a synthetic peptide (CG 117-136) of human lysosomal cathepsin G is dependent on arginine content, Infect. Immun. 64 (1996) 4842–4845.
[13] H.R. Ibrahim, U. Thomas, A. Pellegrini, A helix–loop–helix peptide at the upper lip of the active site cleft of lysozyme confers potent antimicrobial activity with membrane permeabilization action, J. Biol. Chem. 276 (2001) 43767–43774.
[14] A. Pellegrini, U. Thomas, P. Wild, E. Schraner, R. von Fellenberg, Effect of lysozyme or modified lysozyme fragments on DNA and RNA synthesis and membrane permeability of *Escherichia coli*, Microbiol. Res. 155 (2000) 69–77.
[15] K. During, P. Porsch, A. Mahn, O. Brinkmann, W. Gieffers, The non-enzymatic microbicidal activity of lysozymes, FEBS Lett. 449 (1999) 93–100.
[16] H.R. Ibrahim, On the novel catalytically-independent antimicrobial function of hen egg-white lysozyme: a conformation-dependent activity, Nahrung 42 (1998) 187–193.

[17] Y. Mine, F. Ma, S. Lauriau, Antimicrobial peptides released by enzymatic hydrolysis of hen egg white lysozyme, J. Agric. Food Chem. 52 (2004) 1088–1094.
[18] D. Wade, J. Silberring, R. Soliymani, S. Heikkinen, I. Kilpelainen, H. Lankinen, P. Kuusela, Antibacterial activities of temporin A analogs, FEBS Lett. 479 (2000) 6–9.
[19] D. Wade, A. Boman, B. Wahlin, C.M. Drain, D. Andreu, H.G. Boman, R.B. Merrifield, All-D amino acid-containing channel-forming antibiotic peptides, Proc. Natl. Acad. Sci. U. S. A. 87 (1990) 4761–4765.
[20] M.B. Strom, O. Rekdal, J.S. Svendsen, The effects of charge and lipophilicity on the antibacterial activity of undecapeptides derived from bovine lactoferricin, J. Pept. Sci. 8 (2002) 36–43.
[21] E.A.G. Aniansson, S.N. Wall, M. Almgren, H. Hoffman, I. Kielmann, W. Ulbricht, R. Zana, J. Lang, C. Tondre, Theory of the kinetics of micellar equilibria and quantitative interpretation of chemical relaxation studies of micellar solutions of ionic surfactants, J. Phys. Chem. 80 (1976) 905–922.
[22] J.R. Lakowicz, Principles of fluorescence spectroscopy, Kluwer Academic, New York, 1999.
[23] T. Wieprecht, O. Apostolov, M. Beyermann, J. Seelig, Interaction of a mitochondrial presequence with lipid membranes: role of helix formation for membrane binding and perturbation, Biochemistry 39 (2000) 15297–15305.
[24] E.J. Prenner, R.N. Lewis, L.H. Kondejewski, R.S. Hodges, R.N. McElhaney, Differential scanning calorimetric study of the effect of the antimicrobial peptide gramicidin S on the thermotropic phase behavior of phosphatidylcholine, phosphatidylethanolamine and phosphatidylglycerol lipid bilayer membranes, Biochim. Biophys. Acta 1417 (1999) 211–223.
[25] T.L. Hwang, A.J. Shaka, Water suppression that works. Excitation sculpting using arbitrary wave-forms and pulsed-field gradients, J. Magn. Reson., A 112 (1995) 275–279.
[26] B.A. Johnson, R.A. Blevins, NMRView: a computer program for the visualization and analysis of NMR data, J. Biomol. NMR 4 (1994) 603–614.
[27] K. Wuthrich, NMR of proteins and nucleic acids, John Wiley & Sons, Inc., New York, 1986.
[28] A.T. Brunger, P.D. Adams, G.M. Clore, W.L. DeLano, P. Gros, R.W. Grosse-Kunstleve, J.S. Jiang, J. Kuszewski, M. Nilges, N.S. Pannu, R.J. Read, L.M. Rice, T. Simonson, G.L. Warren, Crystallography and NMR system: a new software suite for macromolecular structure determination, Acta Crystallogr., D Biol. Crystallogr. 54 (Pt 5) (1998) 905–921.
[29] M. Nilges, Calculation of protein structures with ambiguous distance restraints. Automated assignment of ambiguous NOE crosspeaks and disulphide connectivities, J. Mol. Biol. 245 (1995) 645–660.
[30] M. Nilges, S.I. O'Donoghue, Ambiguous NOEs and automated NOE assignment, Prog. NMR Spectrosc. 32 (1998) 107–115.
[31] J.P. Linge, M. Nilges, Influence of non-bonded parameters on the quality of NMR structures: a new force field for NMR structure calculation, J. Biomol. NMR 13 (1999) 51–59.
[32] R.A. Laskowski, M.W. MacArthur, D.S. Moss, J.M. Thornton, PROCHECK: a program to check the stereochemical quality of protein structures, J. Appl. Crystallogr. 26 (1993) 283–291.
[33] A.L. Morris, M.W. MacArthur, E.G. Hutchinson, J.M. Thornton, Stereochemical quality of protein structure coordinates, Proteins 12 (1992) 345–364.
[34] R. Koradi, M. Billeter, K. Wuthrich, MOLMOL: a program for display and analysis of macromolecular structures, J. Mol. Graph. 14 (1996) 51–55.
[35] C.B. Park, H.S. Kim, S.C. Kim, Mechanism of action of the antimicrobial peptide buforin II: buforin II kills microorganisms by penetrating the cell membrane and inhibiting cellular functions, Biochem. Biophys. Res. Commun. 244 (1998) 253–257.
[36] C.B. Park, K.S. Yi, K. Matsuzaki, M.S. Kim, S.C. Kim, Structure-activity analysis of buforin II, a histone H2A-derived antimicrobial peptide: the proline hinge is responsible for the cell-penetrating ability of buforin II, Proc. Natl. Acad. Sci. U. S. A. 97 (2000) 8245–8250.
[37] S.J. Opella, NMR and membrane proteins, Nat. Struct. Biol. 4 (1997) 845–848 (Suppl.).
[38] G.D. Henry, B.D. Sykes, Methods to study membrane protein structure in solution, Methods Enzymol. 239 (1994) 515–535.
[39] D.S. Wishart, B.D. Sykes, F.M. Richards, The chemical shift index: a fast and simple method for the assignment of protein secondary structure through NMR spectroscopy, Biochemistry 31 (1992) 1647–1651.
[40] M. Nilges, M.J. Macias, S.I. O'Donoghue, H. Oschkinat, Automated NOESY interpretation with ambiguous distance restraints: the refined NMR solution structure of the pleckstrin homology domain from beta-spectrin, J. Mol. Biol. 269 (1997) 408–422.
[41] D.J. Schibli, P.M. Hwang, H.J. Vogel, Structure of the antimicrobial peptide tritrpticin bound to micelles: a distinct membrane-bound peptide fold, Biochemistry 38 (1999) 16749–16755.
[42] A.S. Ladokhin, S.H. White, Folding of amphipathic alpha-helices on membranes: energetics of helix formation by melittin, J. Mol. Biol. 285 (1999) 1363–1369.
[43] K. Lohner, in: K. Lohner (Ed.), Development of Novel Antimicrobial Agents: Emerging Strategies, Horizon Scientific Press, Oxford, 2001.
[44] R.L. Biltonen, D. Lichtenberg, The use of differential scanning calorimetry as a tool to characterize liposome preparations, Chem. Phys. Lipids 64 (1993) 129–142.
[45] H.A. Rinia, J.W. Boots, D.T. Rijkers, R.A. Kik, M.M. Snel, R.A. Demel, J.A. Killian, J.P. Der Eerden, B. de Kruijff, Domain formation in phosphatidylcholine bilayers containing transmembrane peptides: specific effects of flanking residues, Biochemistry 41 (2002) 2814–2824.
[46] A. Latal, G. Degovics, R.F. Epand, R.M. Epand, K. Lohner, Structural aspects of the interaction of peptidyl–glycylleucine–carboxyamide, a highly potent antimicrobial peptide from frog skin, with lipids, Eur. J. Biochem. 248 (1997) 938–946.
[47] K. Lohner, A. Latal, R.I. Lehrer, T. Ganz, Differential scanning microcalorimetry indicates that human defensin, HNP-2, interacts specifically with biomembrane mimetic systems, Biochemistry 36 (1997) 1525–1531.
[48] H. Heerklotz, J. Seelig, Titration calorimetry of surfactant–membrane partitioning and membrane solubilization, Biochim. Biophys. Acta 1508 (2000) 69–85.
[49] T. Wieprecht, O. Apostolov, M. Beyermann, J. Seelig, Membrane binding and pore formation of the antibacterial peptide PGLa: thermodynamic and mechanistic aspects, Biochemistry 39 (2000) 442–452.
[50] G. Schwarz, S. Stankowski, V. Rizzo, Thermodynamic analysis of incorporation and aggregation in a membrane: application to the pore-forming peptide alamethicin, Biochim. Biophys. Acta 861 (1986) 141–151.
[51] T. Wieprecht, O. Apostolov, M. Beyermann, J. Seelig, Thermodynamics of the alpha–helix–coil transition of amphipathic peptides in a membrane environment: implications for the peptide–membrane binding equilibrium, J. Mol. Biol. 294 (1999) 785–794.
[52] P. Casteels, P. Tempst, Apidaecin-type peptide antibiotics function through a non-poreforming mechanism involving stereospecificity, Biochem. Biophys. Res. Commun. 199 (1994) 339–345.
[53] Y. Shai, Molecular recognition between membrane-spanning polypeptides, Trends Biochem. Sci. 20 (1995) 460–464.
[54] D. Derossi, S. Calvet, A. Trembleau, A. Brunissen, G. Chassaing, A. Prochiantz, Cell internalization of the third helix of the Antennapedia homeodomain is receptor-independent, J. Biol. Chem. 271 (1996) 18188–18193.
[55] Y.R. Chan, R.L. Gallo, PR-39, a syndecan-inducing antimicrobial peptide, binds and affects p130(Cas), J. Biol. Chem. 273 (1998) 28978–28985.